Journal of Solid State Chemistry 182 (2009) 209–214

Contents lists available at ScienceDirect

Journal of Solid State Chemistry

journal homepage: www.elsevier.com/locate/jssc

Ab-initio structure determination of β-La_2WO_6

M-H. Chambrier [a], S. Kodjikian [a], R.M. Ibberson [b], F. Goutenoire [a,*]

[a] Laboratoire des Oxydes et Fluorures, UMR-CNRS 6010, Université du Maine, 72085 Le Mans Cedex 9, France
[b] ISIS Facility, STFC Rutherford Appleton Laboratory, Harwell Science and Innovation Campus, Didcot OX11 0QX, UK

ARTICLE INFO

Article history:
Received 12 March 2008
Received in revised form
5 September 2008
Accepted 9 September 2008
Available online 1 October 2008

Keywords:
Oxide
X-ray and neutron diffraction
Electron microscopy

ABSTRACT

The structure of the low-temperature form of β-La_2WO_6 has been determined from laboratory X-ray, neutron time-of-flight and electron diffraction data. This tungstate crystallizes in the non-centrosymmetric orthorhombic space group (no. 19) $P2_12_12_1$, with $Z=8$, $a=7.5196(1)$ Å, $b=10.3476(1)$ Å, $c=12.7944(2)$ Å, and a measured density 7.37(1) g cm^{-3}. The structure consists of tungsten [WO_6] octahedra and tetrahedral [OLa_4]. Tungsten polyhedra are connected such that $[W_2O_{11}]^{10-}$ units are formed.

1. Introduction

Oxides of the formula Ln_2MO_6 [M = Mo or W] have been the subject of several crystallographic studies (see Table 1) and these compounds typically present structural variants based on the fluorite (CaF_2) or scheelite ($CaWO_4$) structural types. β-La_2WO_6, the low-temperature form of La_2WO_6, has been reported previously by Yoshimura and Rouanet [1] and also by Yanoskii and Voronkova [2]; however, no crystallographic information concerning its structure was given.

2. Experimental

Room temperature and the high-temperature X-ray diffraction patterns were collected on a Bragg–Brentano diffractometer (MPD-PRO Panalytical) with Cobalt radiation equipped with a linear detector X'Cellerator and an Anton Paar HTK12 furnace. The high-temperature X-ray diffraction patterns were collected during one night, from [5°–70°, 2θ], for 30, 200, 400, 800 and 1000 °C. Neutron diffraction data were collected on the high-resolution powder diffractometer, HRPD, at the ISIS pulsed neutron source, Rutherford Appleton Laboratory, UK. Data collection was performed on ~15 g of compound at room temperature.

The electron diffraction study was performed on a 200 kV side entry JEOL2010 transmission electron microscope with a double-tilt specimen holder operating at room temperature. The sample was prepared by grinding a small amount of powder in an agate mortar and pestle under dry 1-butanol to produce a suspension. A drop of the suspension was deposited on a holey carbon film supported by a 1000 mesh copper grid and dried.

The density measurement was performed on a gas picnometer ACCUPIC 1330 (Micromeritics) with helium as gas using approximately 2 g of sample. The temperature of measurement was 24 ± 1 °C.

Transport properties were studied by impedance spectroscopy using a Schlumberger Solartron SI 1260 frequency response analyzer with 0.1 V amplitude signal over the 32 MHz–0.1 Hz frequency range. A 5 mm diameter pellet was used for the measurements with, as electrodes, platinum deposited by sputtering on both faces.

3. Results and discussion

3.1. Synthesis

The compound was prepared with La_2O_3 and WO_3 as starting oxides. Lanthanum oxide powder was dried and decarbonated at 1000 °C overnight prior to use. The oxides were weighed in stochiometric proportions with a 1:1 the molar ration of La_2O_3 and WO_3, and ground together in an agate mortar. The prepared composition was heated up to 1400 °C for one night in an alumina crucible, no particular condition was used in order to cool down the samples. The final compound was white.

The X-ray diffraction pattern was rather similar to those previously study by Yoshimura and Rouanet [1] with the JCPDF reference (00-031-0675). The synthesis of a pure compound is

* Corresponding author. Fax: +33 2 43 83 35 06.
E-mail address: francois.goutenoire@univ-lemans.fr (F. Goutenoire).

0022-4596/$ - see front matter © 2008 Elsevier Inc. All rights reserved.
doi:10.1016/j.jssc.2008.09.010

rather difficult. As mentioned in the phase diagram studies [3], the different compounds occurring in this phase field do not present any notable solid solution (Fig. 1). Thus, the appearance of the two compounds around the composition La_2WO_6 is common. At lower WO_3 molar fractions, $La_6W_2O_{15}$ (JCPDF 00-031-0674) was observed and for the upper molar fractions $La_{14}W_8O_{45}$ (JCPDF 00-032-0502) was observed. $La_6W_2O_{15}$ presents three crystallographic forms α, β and γ, above 930 °C, between 930 and 620 °C and below 620 °C, respectively. None of the structures of these crystallographic forms have been determined. We are currently working on the high-temperature form α-$La_6W_2O_{15}$, which presents orthorhombic cell parameters. The two other lower-temperature forms present significantly more complex crystallographic structures, and are still unknown. The cell parameters for $La_{14}W_8O_{45}$ have been determined previously by Yanoskii and Voronkova [2]; however, the authors have wrongly attributed these cell parameters to La_2WO_6. We have also confirmed the cell parameters of $La_{14}W_8O_{45}$ using electron diffraction and X-ray diffraction. The real composition of this compound is $La_{18}W_{10}O_{57}$, and details of the structure will be published soon. Thus, we choose a composition slightly in excess of WO_3 (50.1 mol% WO_3), in order to have $La_{14}W_8O_{45}$ and not γ-$La_6W_2O_{15}$ as the secondary phase.

Table 1
Crystallographic parameters (cell and space group) for different compounds of formula Ln_2MO_6 (Ln = lanthanide and M = Mo or W)

Formula	a (Å)	b (Å)	c (Å)	β (°)	Z	Space group
La_2MoO_6 [20]	4.089	4.089	15.99	–	2	$I\bar{4}2\,m$
Nd_2MoO_6 [21]	5.658	5.658	31.586	–	8	$I4_1/acdZ$
Er_2MoO_6 [22]	16.325	10.986	5.331	108.62	8	$C12/c1$
Nd_2WO_6 [23]	5.536	9.231	10.170	–	4	$P2_12_12_1$
Nd_2WO_6 [24]	15.920	11.390	5.508	–	8	$I12/c1$
La_2WO_6	7.520	10.348	12.794		8	$P2_12_12_1$

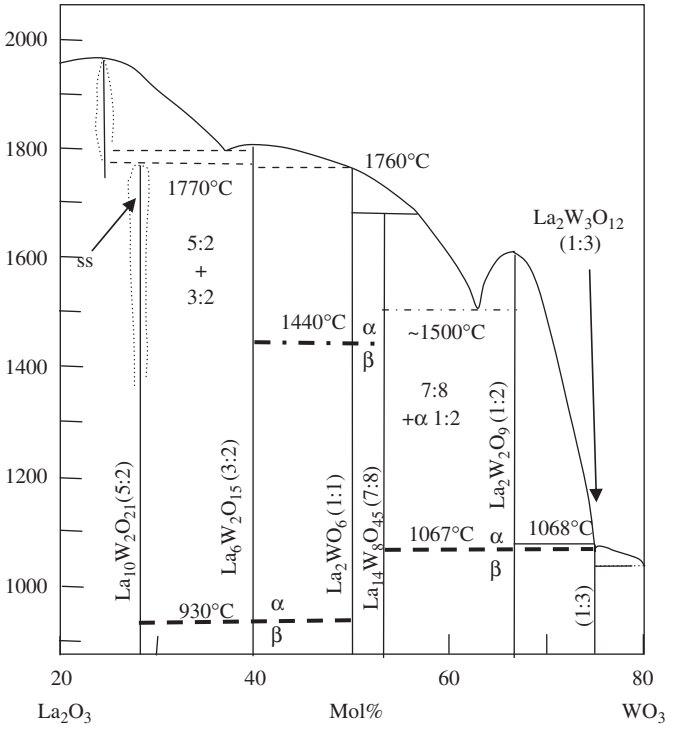

Fig. 1. Phase equilibrium diagram for the system La_2O_3–WO_3 from Ref. [1].

Table 2
Crystallographic parameters of β-La_2WO_6 T.O.F neutron refinement

Atom	x	y	z	U_{iso} (× 100)
La1	0.5666(2)	0.5835(2)	0.4123(2)	0.4(1)
La2	0.7377(2)	0.0552(2)	0.8630(2)	0.6(1)
La3	0.7381(2)	0.5459(2)	0.6736(2)	0.7(1)
La4	0.4787(3)	0.2217(2)	0.5843(2)	2.0(1)
W1	0.5499(4)	0.2294(3)	0.3198(2)	0.2(1)
W2	0.9688(4)	0.1234(3)	0.1279(2)	0.2(1)
O1	0.4738(3)	0.2005(2)	0.9196(2)	0.5(1)
O2	0.0241(3)	0.4384(3)	0.7318(2)	1.4(1)
O3	0.5011(4)	0.2920(3)	0.1813(2)	1.0(1)
O4	0.0309(3)	0.0546(3)	0.4319(2)	0.2(1)
O5	0.0457(3)	0.4572(2)	0.2956(2)	0.6(1)
O6	0.3215(4)	0.3058(3)	0.7526(2)	0.5(1)
O7	0.2502(3)	0.4101(2)	0.9477(2)	0.3(1)
O8	0.3514(4)	0.2475(3)	0.3855(2)	2.0(1)
O9	0.0979(3)	0.0484(3)	0.0201(2)	0.5(1)
O10	−0.1816(4)	−0.3467(3)	0.3000(2)	1.4(1)
O11	0.1732(3)	0.3439(3)	0.5649(2)	0.6(1)
O12	0.1733(3)	0.1161(3)	0.6481(2)	0.5(1)

Bank 1 ($2\theta = 168°$): 1604 reflections, $R_{Bragg} = 7.91\%$, $R_{wp} = 10.6\%$, Bank 2 ($2\theta = 90°$): 638 reflections, $R_{Bragg} = 4.14\%$, $R_{wp} = 6.1\%$.
Space group $P2_12_12_1$ (no. 19), $a = 7.5196(1)$ Å; $b = 10.3476(1)$ Å, $c = 12.7944(2)$ Å, $Z = 8$, Calculated density = 7.44 g cm^{-3}, measured density = 7.37(1) g cm^{-3}.

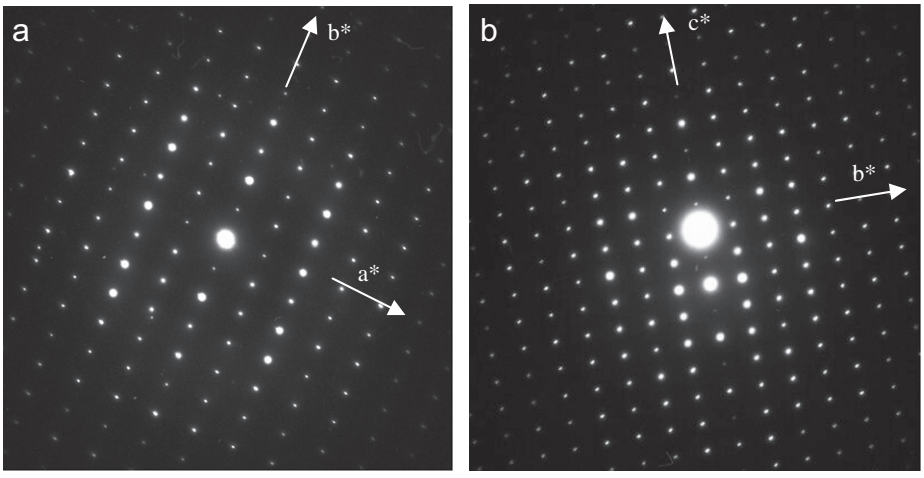

Fig. 2. Electron diffraction patterns of La_2WO_6: (a) along [001]* and (b) [100]*.

3.2. Electron diffraction microscopy

The electron diffraction analysis performed on different crystallites shows sharp spots indicating that our compound is well crystallized. The reciprocal lattice reconstruction, performed by electron diffraction allowed us to determine the cell parameters: $a \approx 7.5$ Å, $b \approx 10.4$ Å, $c \approx 12.8$ Å.

The electron diffraction patterns of the two basal planes could be indexed with the previous parameters. No specific reflection conditions were observed in both electron diffraction patterns or on the reciprocal lattice reconstructions leading to the assignment of a primitive lattice.

We note weak (h00), (0k0), (00l) reflections with h, k, $l = 2n$. These weak reflections are observed on electron diffraction pattern due to the double reflection effect. We can suppose there are three two-fold screw axes along $\vec{a}, \vec{b}, \vec{c}$ (Fig. 2).

3.3. Crystal symmetry

From the analysis of the X-ray powder diffraction data collected on the MPD-PRO, we were able to obtain a good solution from two different autoindexing programs Treor [4] and Dicvol [5] implemented in X'Pert High Score Plus [6]. The solution determined by Treor was: $a = 12.78$ Å, $b = 10.33$ Å, $c = 7.51$ Å, with a figure of merit $M_{20} = 193$ [7]. From the density measurement, $Z = 8$ was deduced from this unit volume cell, giving the contents of the cell as $La_{16}W_8O_{24}$.

All primitive orthorhombic space groups were tested with Le Bail Fit [8] implement in the Fullprof program [9]. The best fit was obtained with the non-centrosymmetric space group $P2_12_12_1$ (no. 19), and this result is in agreement with the electron microscopy analysis.

3.4. Crystal structure determination

In a first step, only the cation positions were sought. The solution was determined by Monte Carlo analysis performed by the program Espoir [10], using only the first 65 peaks. Distance constraints were used between La–W < 3.3 Å, La–La < 3.7 Å and

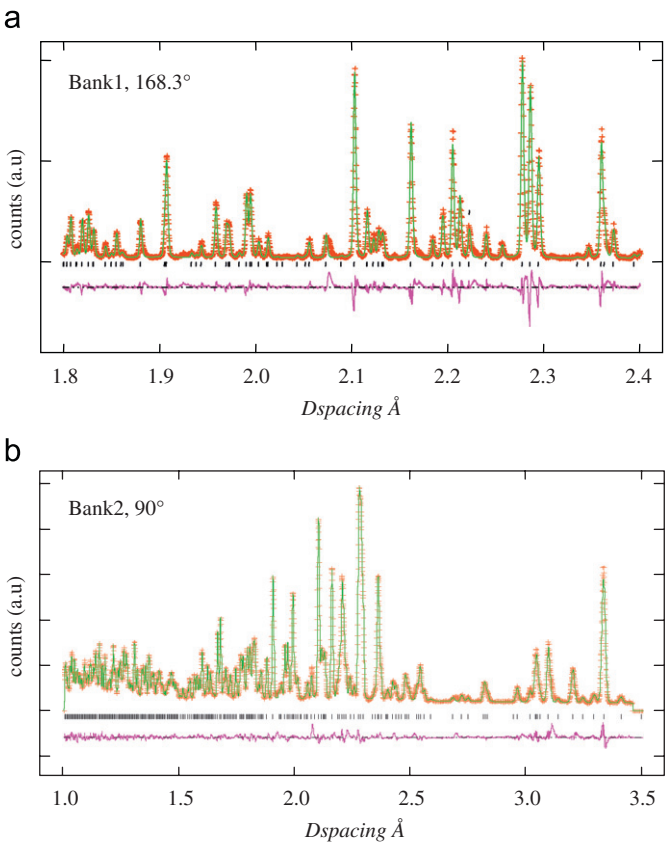

Fig. 3. Results of the final T.O.F profile refinement of La_2WO_6, observed cross, calculated line and difference lower profiles are shown: (a) bank 1 and (b) bank 2.

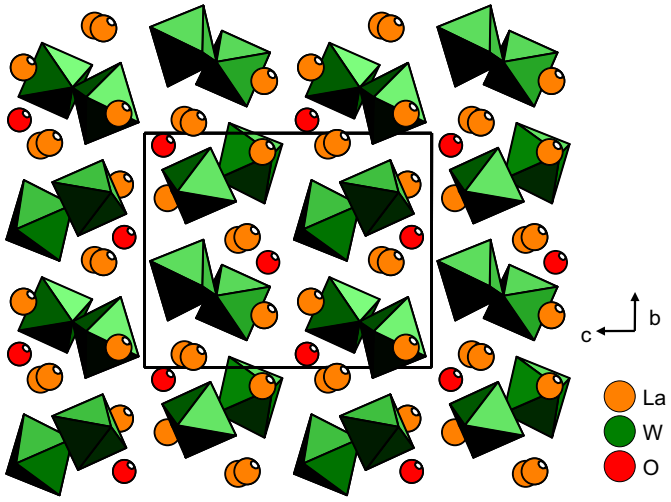

Fig. 5. Projection of La_2WO_6 structure along [100].

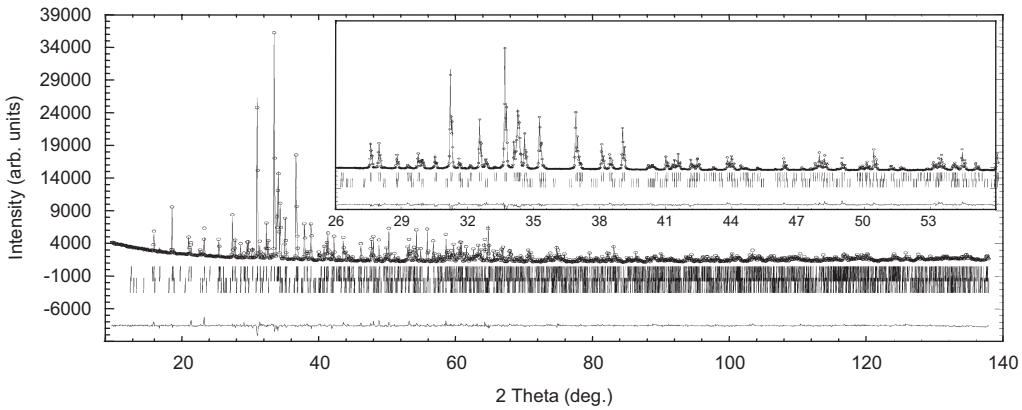

Fig. 4. Final X-ray profile refinement of La_2WO_6, observed cross, calculated line and difference lower profiles are shown. *Inset*: expanded view of the $2\theta = 26$–56° region.

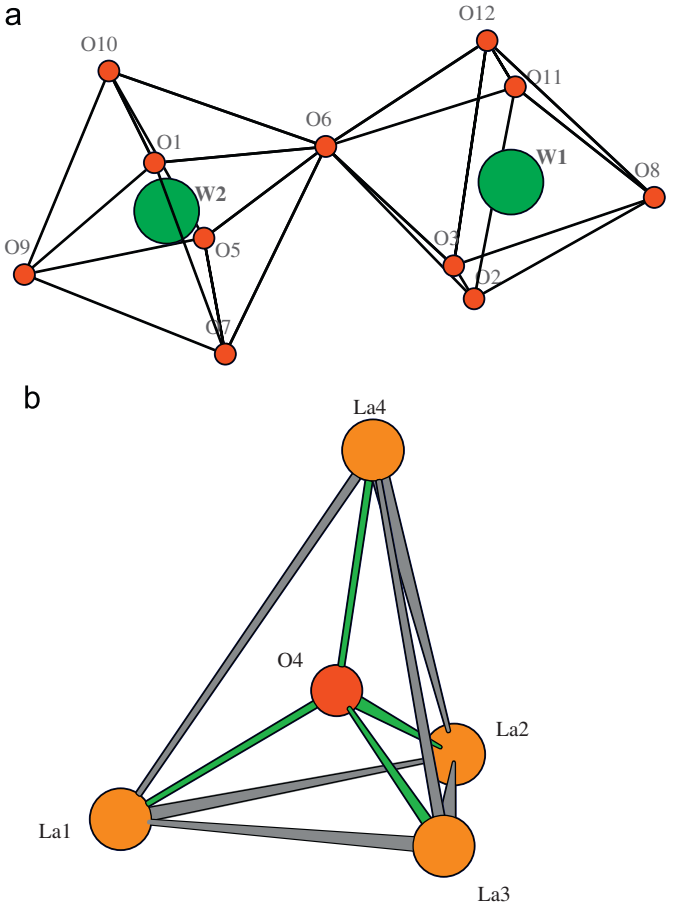

Fig. 6. (a) Detail of the $[W_2O_{11}]^{-10}$ structural unit formed by two corner-sharing octahedra. (b) Detail of the $[OLa_4]^{+10}$ structural unit.

W–W < 3.3 Å, in order to help in the search of these atomic positions. Rapidly, a good solution was obtained, $R = 8.2\%$, after 10 h of calculation. The first nine oxygen atomic positions were subsequently found after Fourier difference analysis and Rietveld refinement. The positions of the remaining three oxygen atoms were only found with the help of the neutron data.

3.5. Refinement and structure analysis

The whole neutron powder patterns were used in order to refine the previous structural model coming from the X-ray structural determination using the Rietveld method implemented by GSAS [11]. To fit the neutron data, refinement of an absorption coefficient was required in order to avoid small negative thermal parameters observed initially for some atoms. A combined X-ray neutron refinement was tested without success. The final atomic positions and atomic displacement factors refined from data recorded using both backscattering ($\langle 2\theta \rangle = 168^\circ$) and 90° detector banks are reported in Table 2a with the corresponding reliability factors. The final profile fit is presented in Fig. 3a and b. For comparison, the atomic positions and atomic displacement factors refined from the X-ray diffraction data are also listed in supplementary information. The negative atomic displacement factor obtained for the tungsten positions is obviously spurious and it is most likely due to correlation with parameters modeling the background at high angle. Nevertheless the X-ray refinement gives some good reliability factors $R_{Bragg} = 8.51\%$ and $R_{wp} = 13.7\%$, the result is presented in Fig. 4. The secondary $La_{14}W_8O_{45}$ phase observed in this diagram was treated as an impurity in the refinement. The integrated peak intensities of $La_{14}W_8O_{45}$ were extracted from the powder X-ray pattern of pure $La_{14}W_8O_{45}$, by a full pattern decomposition method in the range $10^\circ \leqslant 2\theta \leqslant 110^\circ$. During the refinement, the relative intensities were fixed and only three parameters a, c and the scale factor, were refined ($a = 9.036$ Å, $c = 32.557$ Å, $P6_3/mmc$).

Table 3
Bond distances between W-O in the diagonal in italic format and in the upper place the oxygen-oxygen distances (Å) and bond angles between O-W-O atoms in the lower place for β-La_2WO_6 derived from neutron analysis

W1	O2	O3	O6	O8	O11	O12
O2	*1.868(3)* Å	*2.636(3)* Å	*2.638(3)* Å	*2.764(4)* Å	*2.603(4)* Å	*2.819(3)* Å
O3	88.1(2)°	*1.923(3)* Å	*2.747(3)* Å	*2.882(4)* Å	–	*2.710(3)* Å
O6	78.5(2)°	81.3(2)°	*2.273(4)* Å	–	*2.678(4)* Å	*2.623(3)* Å
O8	100.5(2)°	104.3(2)°	174.2(2)°	*1.723(4)* Å	*2.674(3)* Å	*2.835(3)* Å
O11	87.4(2)°	160.6(2)°	79.3(2)°	95.0(2)°	*1.900(4)* Å	*2.586(3)* Å
O12	155.8(2)°	90.5(2)°	77.5(2)°	103.2(2)°	86.0(2)°	*1.893(3)* Å

W2	O1	O5	O6	O7	O9	O10
O1	*1.921(3)* Å	*3.246(3)* Å	*2.658(3)* Å	*2.768(3)* Å	*2.867(3)* Å	*2.660(3)* Å
O5	168.6(2)°	*1.982(3)* Å	*2.705(3)* Å	2.834(3)Å	2.759(3)Å	*2.653(30)* Å
O6	84.6(2)°	84.9(2)°	*2.025(3)* Å	*2.772(3)*Å	–	*2.806(3)*Å
O7	91.6(2)°	92.6(2)°	88.7(2)°	*1.938(3)* Å	*2.682(3)*Å	–
O9	98.7(2)°	91.9(2)°	176.4(2)°	89.9(2)°	*1.856(3)* Å	*2.621(3)*Å
O10	89.0(2)°	86.9(2)°	92.0(2)°	179.1(2)°	89.3(2)°	*1.873(4)* Å

La1–O1: 2.487(3)	La2–O1: 2.593(3)	La3–O1: 2.554(3)	La4–O4: 2.357(3)
La1–O2: 2.418(3)	La2–O2: 2.478(3)	La3–O2: 2.533(3)	La4–O5: 2.458(3)
La1–O3: 2.520(3)	La2–O3: 2.595(3)	La3–O3: 2.583(3)	La4–O6: 2.606(3)
La1–O4: 2.468(3)	La2–O4: 2.480(3)	La3–O4: 2.308(3)	La4–O8: 2.731(3)
La1–O7: 2.426(3)	La2–O5: 2.495(2)	La3–O5: 2.644(3)	La4–O8: 2.847(3)
La1–O9: 2.691(3)	La2–O7: 2.450(3)	La3–O6: 2.886(3)	La4–O9: 2.970(3)
La1–O10: 2.483(3)	La2–O11: 2.466(3)	La3–O9: 2.768(2)	La4–O11: 2.634(3)
La1–O12: 2.347(3)		La3–O10: 2.654(3)	La4–O11: 2.499(3)
		La3–O12: 2.486(3)	La4–O12: 2.671(3)

Table 4
Calculated bond valence for β-La_2WO_6

Atom	Calculated bond valence	Atom	Calculated bond valence
La1	3.5(1)	O4	2.2(1)
La2	2.9(1)	O5	2.0(1)
La3	3.1(1)	O6	1.6(1)
La4	2.8(1)	O7	1.9(1)
W1	6.3(3)	O8	2.1(2)
W2	5.9(2)	O9	1.7(1)
O1	2.1(1)	O10	1.8(1)
O2	2.5(1)	O11	2.2(1)
O3	2.0(1)	O12	2.4(1)

$B = 0.37$ Å, $Ro(La^{3+}–O^{2-}) = 2.172$ Å and for $Ro(W^{6+}–O^{2-}) = 1.921$ Å.

Bond valence calculations were performed directly by the program Bond Str [9] with the atomic position deduced from the neutron refinement, using the Brown–Altermatt empirical expression: valence $= \Sigma\exp(Ro\text{-}d)/B$ with $B = 0.37$ Å [12]. The results of the bond valence calculations for each atom type give values around the expected +3, +6 and −2 (see Table 4) for lanthanum, tungsten and oxygen, respectively. The discrepancy between calculated and theoretical values does not exceed 23%, this maximum is found for O2.

The projection of the structure along [100] is presented in Fig. 5. The main feature of interest in the structure is the formation of a block unit of formula $[W_2O_{11}]^{-10}$ resulting from a corner-sharing of two octahedra (Fig. 6a). The structure of β-La_2WO_6 can then be described by one $[W_2O_{11}]^{-10}$ plus one $[OLa_4]^{+10}$. This latter unit is made with the only oxygen atom which is not bonded to a tungsten atom, namely O4. This oxygen is surrounded by the four lanthanum atoms at distances ranging 2.308–2.480 Å (Table 3), forming distorted tetrahedra (Fig. 6b). The four lanthanum atoms La1, La2, La3 and La4 are connected to oxygen atoms O8, O7, O9 and O9, respectively.

The formation of corner-sharing tetrahedra, trigonal bipyramids and octahedra is usual in a number of molybdates or tungstates [13–16]. We note also in the same phase diagram that units of $[W_4O_{18}]^{-12}$, formed by two octahedra plus two trigonal bipyramids sharing corners, occur in the low-temperature formof β-$La_2W_2O_9$ [16] (Fig. 7).

3.6. Impedance and thermal expansion measurements

The La_2O_3–MoO_3 or La_2O_3–WO_3 phase diagram contains a number of compounds with interesting ionic conduction and thermal expansion properties, for example, the fast ion conductor $La_2Mo_2O_9$ [17] and $Y_2Mo_3O_{12}$ [18] for the thermal expansion behavior. Accordingly these properties were investigated in β-La_2WO_6.

The Nyquist plot of β-La_2WO_6 does not show Warburg behavior at low frequency; similar behavior is observed for $La_6Mo_8O_{33}$ in the La_2O_3–MoO_3 system. The observation of Warburg behavior is typically associated with good ionic conductors and since the impedance measured at 700 °C is of the same order as $La_6Mo_8O_{33}$, around $10^6\,\Omega$ we can conclude that β-La_2WO_6 does not exhibit any ionic conduction.

The coefficient of thermal expansion was measured by means of high-temperature X-ray diffraction. The calculated thermal expansion coefficient $\alpha_{30,1000}$ is $11.6\times10^{-6}\,^\circ K^{-1}$ which is comparable with $La_7Nb_3W_4O_{30}$ $\alpha_{30,1000} = 11.2\times10^{-6}\,^\circ K^{-1}$ and $La_2Mo_2O_9$ $\alpha_{30,1000}\approx16\times10^{-6}\,^\circ K^{-1}$ [19]. The linear thermal expansion for each crystallographic direction is rather isotropic $\alpha_1\approx13.7\times10^{-6}\,^\circ K^{-1}$, $\alpha_2\approx10.5\times10^{-6}\,^\circ K^{-1}$, $\alpha_3\approx10.2\times10^{-6}\,^\circ K^{-1}$.

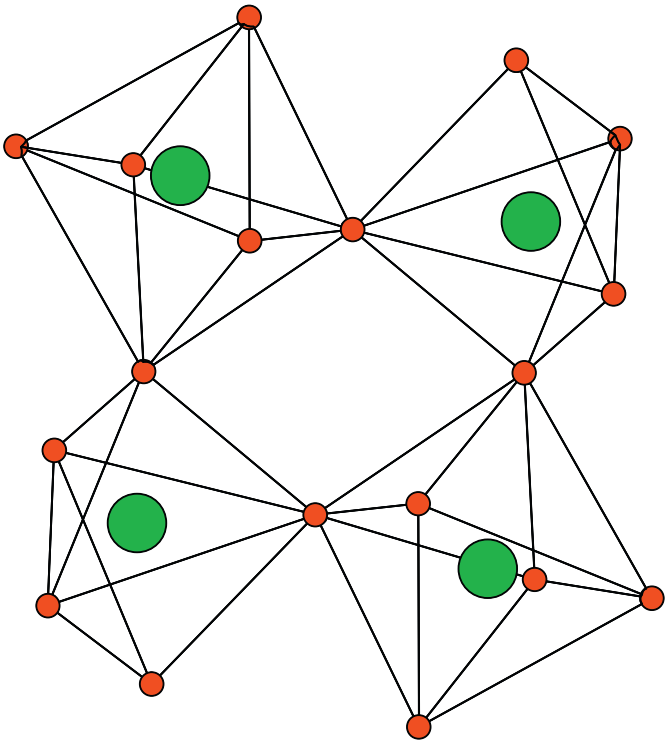

Fig. 7. Coordination polyhedral unit $[W_4O_{18}]^{-12}$ observed in the β-$La_2W_2O_9$ structure formed by corner-sharing of two octahedra plus two trigonal bipyramids.

4. Conclusion

The structure of β-La_2WO_6 has been determined and refined from X-ray and neutron time-of-flight powder diffraction data. The structure comprises $[W_2O_{11}]^{10-}$ and $[OLa_4]^{10+}$ units. Transport properties of La_2WO_6 have been explored by impedance spectroscopy. The compound shows a regular thermal expansion and it does not exhibit any oxide-ion conduction properties.

Appendix A. Supplementary materials

Supplementary data associated with this article can be found in the online version at doi:10.1016/j.jssc.2008.09.010.

References

[1] M. Yoshimura, A. Rouanet, Mater. Res. Bull. 11 (2) (1976) 151–158.
[2] V.K. Yanoskii, V.I. Voronkova, Sov. Phys. Crystallogr. 20 (3) (1975) 354–355.
[3] Acer-Nist, Phase Equilibria Diagram, diagram 93-047.
[4] P.-E. Werner, Z. Kristallogr. 120 (1964) 375–387.
[5] A. Boultif, D. Louër, J. Appl. Cryst. 24 (1991) 987–993.
[6] X'Pert High Score Plus, Producted by PANalytical B.V., Almelo, Netherlands, version 2.0.1, 2004.
[7] P.M. de Wolff, J. Appl. Cryst. 1 (1968) 108.
[8] A. Le Bail, H. Duroy, J.F. Fourquet, Mater. Res. Bull. 23 (1988) 447–452.
[9] J. Rodriguez-Carvajal, Abstrats of the Satellite Meeting on Powder Diffraction of the XV Congress of the IUCr, Toulouse, France, 1990, 127pp.
[10] A. Le Bail, Program Espoir 3.5, 〈http://sdpd.univ-lemans.fr/sppd/espoir/, 2000〉.
[11] A.C. Larson, R.B. Von Dreele, General Structure Analysis System, GSAS, Los Alamos National Laboratory, Los Alamos, NM.
[12] I.D. Brown, D. Altermatt, Acta Crystallogr. B 41 (1985) 244.
[13] F. Dubois, F. Goutenoire, Y. Laligant, E. Suard, P. Lacorre, J. Solid State Chem. 159 (2001) 228–233.
[14] V. Brizé, S. Georges, S. Kodjikian, E. Suard, F. Goutenoire, J. Solid State Chem. 177 (2004) 2617–2627.
[15] Y. Laligant, A. Le Bail, F. Goutenoire, J. Solid State Chem. 159 (2001) 223–227.

[16] H. Naruke, T. Yamase, J Solid State Chem. 173 (2003) 407–417.
[17] P. Lacorre, F. Goutenoire, O. Bohnke, R. Retoux, Y. Laligant, Nature 404 (2000) 856–858.
[18] S.D. Gates, C. Lind, J. Solid State Chem. 180 (12) (2007) 3510–3514.
[19] I.P. Marozau, A.L. Shaula, V.V. Kharton, N.P. Vyshato, A.P. Vishup, J.R. Frade, F.M.B. Marques, Mater. Res. Bull. 40 (2005) 361–371.
[20] L.G. Sillen, K. Lundborg, Z. Anorg. Allg. Chem. 252 (1943) 2–8.
[21] V.A. Efremov, A.V. Tyulin, V.K. Trunov, Koordinatsionnaya Khimiya 13 (1987) 1276–1282.
[22] J.A. Alonso, F. Rivillas, M.J. Martinez-Lope, V. Pomjakushin, J. Solid State Chem. 177 (2004) 2470–2476.
[23] V.A. Efremov, V.A. Tyulin, V.K. Trunov, Kristallografiya 29 (1984) 673–676.
[24] T.M. Polyanskaya, S.V. Borisov, N.V. Belov, Dokl. Akad. Nauk SSSR 193 (1970) 83–86.